

# Chapter 1

## Radio Antennas

Albert Greve

greve@iram.fr

IRAM, 300 rue de la Piscine, F-38406 Saint Martin d'Hères

### 1.1 Introduction

We can define a *radio antenna* as an instrument which *collects*, and *detects*, *electromagnetic radiation* from a certain *area* and *direction* of the sky, allowing to build up an image from individual observations. In radio astronomy we are interested in the detection and analysis of radiation emitted from celestial objects, i.e. solar system bodies, stars, interstellar gas, galaxies, and the universe. The electromagnetic radiation observed in radio astronomy covers the wavelength range from several meters, say 10 m (= 30 MHz), to a fraction of a millimeter, say 0.3 mm ( $\approx 1000$  GHz). Since the antenna must be many wavelengths in diameter in order to collect a large amount of energy and to provide a reasonable directivity (angular resolution), it is evident that antennas for meter wavelengths may have dimensions of many 10 meters to several 100 meters, while antennas for millimeter wavelengths have dimensions of several meters to several 10 meters ( $\approx 10\,000$  to  $50\,000 \lambda$ 's). The technique of mechanical construction is therefore different for meter and millimeter wavelength antennas: antennas for m-wavelengths can be constructed, for instance, as mesh-wire networks and plate arrays, mm-wavelength antennas are full-aperture solid surface parabolic reflector antennas. Typical examples are the obsolete Mills-Cross antenna, the Effelsberg and GBT 100-m antennas, and the IRAM 30-m (Pico Veleta) and 15-m (Plateau de Bure) antennas. However, despite the variety of mechanical constructions, all antennas can be understood from basic principles of electromagnetic radiation, optics, and diffraction.

Here we discuss full-aperture parabolic antennas, like the IRAM antennas, which are used for observations at  $\sim 3 - 0.8$  mm wavelength (100 - 350 GHz). These antennas are very similar to optical reflector telescopes and use in particular the Cassegrain configuration of a parabolic main reflector and a hyperbolic subreflector (Figure 1.3), with an image formed at the secondary focus near the vertex of the main reflector where the receiver, or a receiver-array, is installed. These antennas are steerable and can observe in any direction of the visible hemisphere, with the facility of tracking, scanning, and mapping of a source.

The collected radiation is concentrated in the secondary focus and is (coherently) detected by a receiver at a certain frequency  $\nu$  (or wavelength  $\lambda$ ) and within a certain bandwidth  $\Delta\nu$  (or  $\Delta\lambda$ ). Heterodyne mm-wavelength receivers, which preserve the phase of the incident radiation, have small bandwidths of the order of  $\Delta\nu = 0.5 - 2$  GHz so that  $\Delta\nu/\nu = \Delta\lambda/\lambda \approx 0.5 \text{ GHz}/100 \text{ GHz} \approx 1/200$ . From the point of view of antenna optics, these receivers detect “monochromatic” radiation, and the antenna characteristics can be calculated for a monochromatic wave (as will be done below). Bolometer receivers, on the other hand, detect power in a broad bandwidth of the order of  $\Delta\nu \approx 50$  GHz so that  $\Delta\nu = 50 \text{ GHz}/250 \text{ GHz} \approx 1/5$ . These detectors are no longer monochromatic, and the chromatism of the antenna must be considered in their application.

The construction and operation of a radio antenna is based on exact physical theories, like Maxwell’s theory of electromagnetic radiation, the pointing theory of an astronomical instrument, the transformation (mixing, down-conversion, amplification) and detection of electromagnetic radiation, etc. The theory of a radio antenna presented here is, however, only the very tip of an iceberg (of several 100 000 published pages), but may provide sufficient information for the user astronomer to understand the basic principle of a telescope, either a perfect one, which nobody has but which can be described with high precision, or a real one, with small defects and aberrations, which can be described with sufficient detail to apply corrections.

The theory, construction, and use of radio antennas is contained in many textbooks and journals such as IEEE Transactions Antennas and Propagation, Radio Science, Applied Optics. A biased selection is mentioned here: [Born & Wolf 1975] [Reynolds et al. 1989] [Love 1978] [Lo and Lee] [Kraus 1982] [Goldsmith 1988]

## 1.2 Basic Principles

The properties of electromagnetic radiation propagation and of radio antennas can be deduced from a few basic physical principles, i.e.

1. the notion that Electromagnetic Radiation are Waves of a certain Wavelength ( $\lambda$ ), or Frequency ( $\nu$ ), and Amplitude ( $\mathbf{A}$ ) and Phase ( $\varphi$ );
2. from Huygens Principle which says that each element of a wavefront is the origin of a Secondary Spherical Wavelet;
3. the notion that the Optical Instrument (like a single-dish antenna, a telescope, etc.) combined with a receiver manipulates the incident wavefront through their respective phase and amplitude transfer functions.

Summarized in one sentence, and proven in the following, we may say that the radio antenna transforms the radiation incident on the aperture plane ( $\mathcal{A}$ ) to an image in the image plane ( $\mathcal{I}$ ), also called focal plane. Following Huygens Principle illustrated in Figure 1.1, the point  $\mathbf{a}(x,y) \equiv \mathbf{a}(\vec{r})$  of the incident wavefront in the aperture plane  $\mathcal{A}$  is the origin of a spherical wavelet of which the field  $\delta\mathbf{E}(\mathbf{a}')$  at the point  $\mathbf{a}'(u,v) \equiv \mathbf{a}(\vec{u})$  in the image plane  $\mathcal{I}$  is

$$\delta\mathbf{E}(\vec{u}) = \mathbf{A}(\vec{r})\exp[iks]/s \quad (1.1)$$

with  $k = 2\pi/\lambda$ . The ensemble of spherical wavelets arriving from all points of  $\mathcal{A}$  at the point  $\mathbf{a}'(\vec{u})$  of the image plane  $\mathcal{I}$  produces the field

$$\mathbf{E}(\vec{u}) = \int_{\mathcal{A}} \mathbf{A}(\vec{r})\Lambda(\beta)[\exp(iks)/s]dx dy \quad (1.2)$$

For the paraxial case, when the rays are not strongly inclined against the direction of wave propagation (i.e. the optical axis), the inclination factor  $\Lambda$  can be neglected since  $\Lambda(\beta) \approx \cos(\beta) \approx 1$ . Also,  $s \approx s_0$  for paraxial rays, but  $\exp[iks] \neq \exp[iks_0]$  since these are cosine and sine terms of  $s$  where a small change in

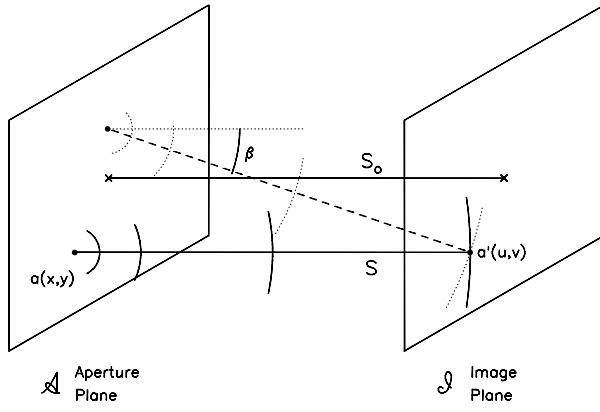


Figure 1.1: Illustration of Huygens Principle. The individual points of the plane wavefront in the aperture plane ( $\mathcal{A}$ ) are the origin of secondary spherical wavelets, which propagate to the right, and superpose to form a plane wavefront in the image plane ( $\mathcal{I}$ ). The optical instrument (telescope) is placed in between  $\mathcal{A}$  and  $\mathcal{I}$ .

$s$  may produce a large change of the cosine or sine value. Thus, for the paraxial approximation we may write

$$s = [(x - u)^2 + (y - v)^2 + z^2]^{1/2} \approx R + g(x, y, R) - (xu + yv)/R \quad (1.3)$$

with

$$R = (x^2 + y^2 + z^2)^{1/2} \quad \text{and} \quad g(x, y, R) = (x^2 + y^2)/2R \quad (1.4)$$

When using these expressions in Eq.1.2, we obtain

$$E(u, v) = [\exp(ikR)/s_0] \int_{\mathcal{A}} A(x, y) \exp[ik(g(x, y, R) - (ux + vy)/R)] dx dy \quad (1.5)$$

This equation describes the paraxial propagation of a wavefront, for instance the wavefront arriving from a very far away star. In particular, this equation says, that without disturbances or manipulations in between  $\mathcal{A}$  and  $\mathcal{I}$  the plane wavefront continues to propagate in straight direction as a plane wavefront.

### 1.3 The perfect Single-Dish antenna

We now place an optical instrument (a mirror, lens, telescope etc.) in the beam between  $\mathcal{A}$  and  $\mathcal{I}$  with the intention, for instance, to form an image of a star. Optical instruments are invented and developed already since several centuries; however, the physical-optics (diffraction) understanding of the image formation started only a good 200 years ago. Thus, speaking in mathematical terms, the telescope ( $\mathcal{T}$ ) manipulates the phases (not so much the amplitudes) between the points ( $\vec{r}$ ) of the aperture plane ( $\mathcal{A}$ ) and the points ( $\vec{u}$ ) of the image plane ( $\mathcal{I}$ ) by the phase transfer function  $\Omega_{\mathcal{O}}(\vec{r}, \vec{u})$ , so that the wavefront converges in the focal point. The receiver ( $\mathcal{R}$ )/detector introduces an additional modulation of the amplitude  $\Omega_{\mathcal{R}}(\vec{r}, \vec{u})$ , as described below. Using this information, the field distribution in the focal plane ( $\mathcal{I}$ ) of the telescope becomes

$$E(\vec{u}) = [\exp(ikR)/s_0] \int_{\mathcal{A}} A(\vec{r}) \Omega_{\mathcal{O}} \Omega_{\mathcal{R}} \exp[ik(g(x, y, R) - (ux + vy)/R)] dx dy \quad (1.6)$$

The phase modulation of the parabolic reflector used in a radio telescope is, fortunately,

$$\Omega_{\mathcal{O}} = \exp[-ik g(x, y, F)] \quad (1.7)$$

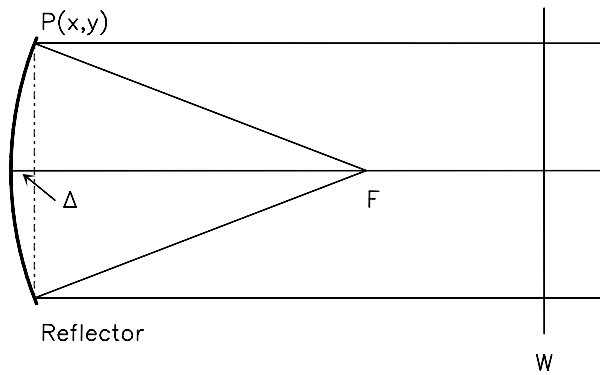


Figure 1.2: Phase modulation of a reflector. The plane wavefront (W) propagates to the left and the ray reflected at P(x,y) toward the focus F is shifted in phase by the amount  $\Delta$ .

(where F is the focal length of the reflector), which inserted into Eq.1.6 eliminates this term in the exponent so that

$$E(\vec{u}) = [\exp(ikF)/F] \int_{\mathcal{A}} A(\vec{r}) \Omega_R \exp[-ik(ux + vy)/F] dx dy \equiv \mathcal{FT}[A(\vec{r}) \Omega_R(\vec{r})] \quad (1.8)$$

This equation says that the field distribution  $E(\vec{u})$  in the focal plane of the telescope is the Fourier transform ( $\mathcal{FT}$ ) of the receiver-weighted field distribution  $A(\vec{r}) \Omega_R(\vec{r})$  in the aperture plane. Since  $E(\vec{u}) E^*(\vec{u}) \neq \delta(\vec{u} - \vec{u}_o)$  for a realistic optical instrument/telescope with limited aperture size, we arrive at the well known empirical fact that the image of a point-like object is not point-like; or, with other words, the image of a star is always blurred by the beam width of the antenna  $\Theta_b \propto \lambda/D$ , with  $D$  the diameter of the reflector.

To close the argumentation, we need to show that the telescope manipulates the incident wave in the way given by Eq.1.7). To demonstrate this property in an easy way, we consider in Figure 1.2 the paraxial rays of a parabolic reflector of focal length F. From geometrical arguments we have

$$(F - \Delta)^2 + (x^2 + y^2) = F^2 \quad (1.9)$$

which for small  $\Delta$  becomes

$$\Delta = -(x^2 + y^2)/F \equiv -g(x, y, F) \equiv \Omega_O(\vec{r}) \quad (1.10)$$

which is the instrumental phase modulation function  $\Omega_O$  used above. The proof is given for a simple parabolic reflector; however, a combined telescope with main reflector and subreflector can be treated in a similar way, leading to the same result.

The fundamental Eq.1.8 can be used to show that an interferometer is *not* a single dish antenna, even though one tries with many individual telescopes and many telescope positions (baselines) to simulate as good as possible the aperture of a large reflector. If we assume for the single dish antennas that  $A(\vec{r}) \equiv 1$  and  $\Omega_R \equiv 1$ , then the power pattern  $P(\vec{u})$  (beam pattern) in the focal plane of the single antenna is

$$P(\vec{u}) = E(\vec{u}) E^*(\vec{u}) = \int_{\mathcal{A}} \int_{\mathcal{A}} \exp[-ik\vec{u}(\vec{x}_1 - \vec{x}_2)] (dx dy)_1 (dx dy)_2 \propto [J_1(\vec{u})/u]^2 \quad (1.11)$$

where  $J_1$  is the Bessel function of first order (see [Born & Wolf 1975]). The function  $[J_1(u)/u]^2$  is called Airy function, or Airy pattern. The interferometer does not simulate a continuous surface, but consists of individual aperture sections  $\mathcal{A}_\infty, \mathcal{A}_\epsilon, \dots$  of the individual telescopes, so that its power pattern  $P_\Sigma(\vec{u})$  (beam pattern) in the focal plane is

$$P_\Sigma(\vec{u}) = \sum_n \sum_m \int_{\mathcal{A}_n} \int_{\mathcal{A}_m} \exp[ik\vec{u}(\vec{x}_1 - \vec{x}_2)] (dx dy)_1 (dx dy)_2 \neq P(\vec{u}) \quad (1.12)$$

The important result of this equation is the fact that the image obtained with the interferometer is “incomplete”, though certainly not as blurred as seen with a single telescope ( $\Theta_D \propto \lambda/D$ ), but having the superior

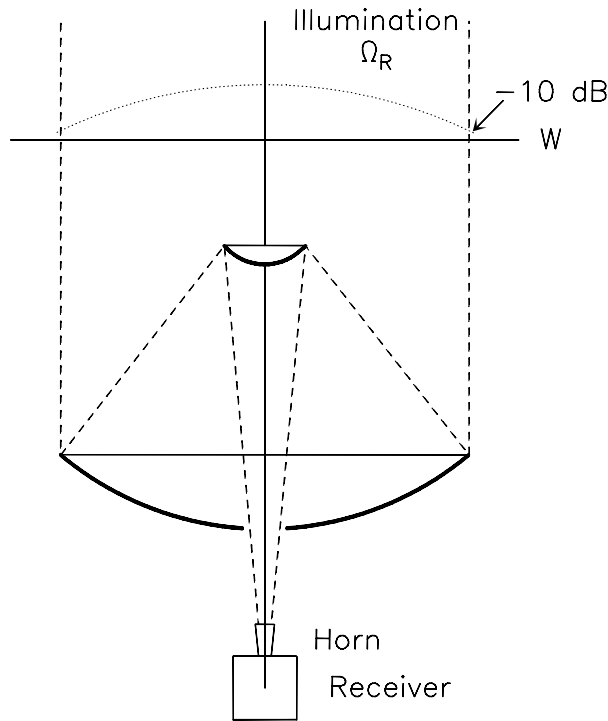


Figure 1.3: The figure shows a Cassegrain telescope and the illumination  $\Omega_R$  of the incident plane wavefront  $W$ .

resolution of the spatial dimension (approximately the longest baseline  $\mathcal{B}$ ) of the array ( $\Theta_B \propto \lambda/\mathcal{B}$ ). For the Plateau de Bure interferometer  $\mathcal{B}/D \approx 300\text{ m}/15\text{ m} \approx 20$  so that  $\Theta_B \approx 1/20 \Theta_D$ . The incompleteness sometimes requires (in particular for mm-VLBI observations which are very similar) additional information for a full image reconstruction, for instance that the object consists of several point-like sources, or a point-like source and a surrounding halo, etc. (see for instance the number of components in CLEAN).

The single telescope selects a part of the incident plane wavefront and 'bends' this plane into a spherical wave which converges toward the focus. This spherical wavefront enters the receiver where it is mixed, down-converted in frequency, amplified, detected, or correlated. The horn-lens combination of the receiver modifies the amplitude of the spherical wavefront in a way expressed by the function  $\Omega_R(\vec{r})$ . This function, called taper or illumination function of the horn-lens combination, weighs the wavefront across the aperture, usually in a radial symmetric way. Figure 1.3 shows, schematically, the effect of a parabolic taper as often applied on radio telescopes, and expressed as

$$\Omega_R(\rho) = K + [1 - \rho^2]^p \quad (1.13)$$

with  $\rho$  the normalized radius of the circular aperture, and  $K$  and  $p$  being constants. For  $A(\vec{r}) \equiv 1$  (i.e. an incident wavefront without structure) the diffraction integral is

$$E_T(\vec{u}) = \int_{\mathcal{A}} \Omega_R(\vec{x}) \exp[-ik\vec{u}\vec{x}] dx dy \quad \text{and} \quad E(\vec{u})E^*(\vec{u}) \equiv A_T(\vec{u}) \quad (1.14)$$

$E_T$  is the tapered field distribution in the focal plane, and  $A_T$  the tapered beam pattern.

Figure 1.4 shows as example a two-dimensional cut through the calculated beam pattern  $A_T$  of the IRAM 15-m telescope at  $\lambda = 3\text{ mm}$ , once without taper (i.e. for  $\Omega_R(\vec{x}) \equiv 1$ ), and for a -10 dB edge taper, i.e. when the weighting of the wavefront at the edge of the aperture is 1/10 of that at the center (see Figure 1.3). As seen from the figure, the taper preserves the global structure of the non-tapered beam pattern, i.e. the main beam and side lobes, but changes the width of the beam (BW:  $\Theta_b$ ), the position of the first null ( $\Theta_{nb}$ ), and the level of the side lobes. The effect of the taper depends on the steepness of the main reflector used in the telescope, as shown in Figure 1.5. The influence of several taper forms is given in Table 1.1 [Christiansen and Hogbom 1969].

The complete telescope, i.e. the optics combined with the receiver, has a beam pattern  $A_T(\vec{u})$  (in optics called point-spread-function) with which we observe point-like or extended objects in the sky

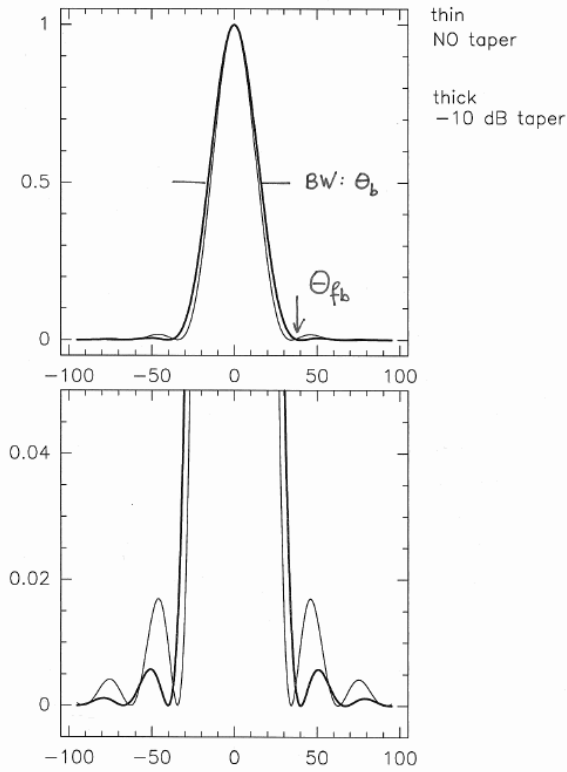


Figure 1.4: The figure shows the calculated beam pattern of the IRAM 15-m telescope at  $\lambda = 3$  mm without taper, and for a -10dB edge taper. The horizontal scale is in arcseconds, the vertical scale is normalized power.

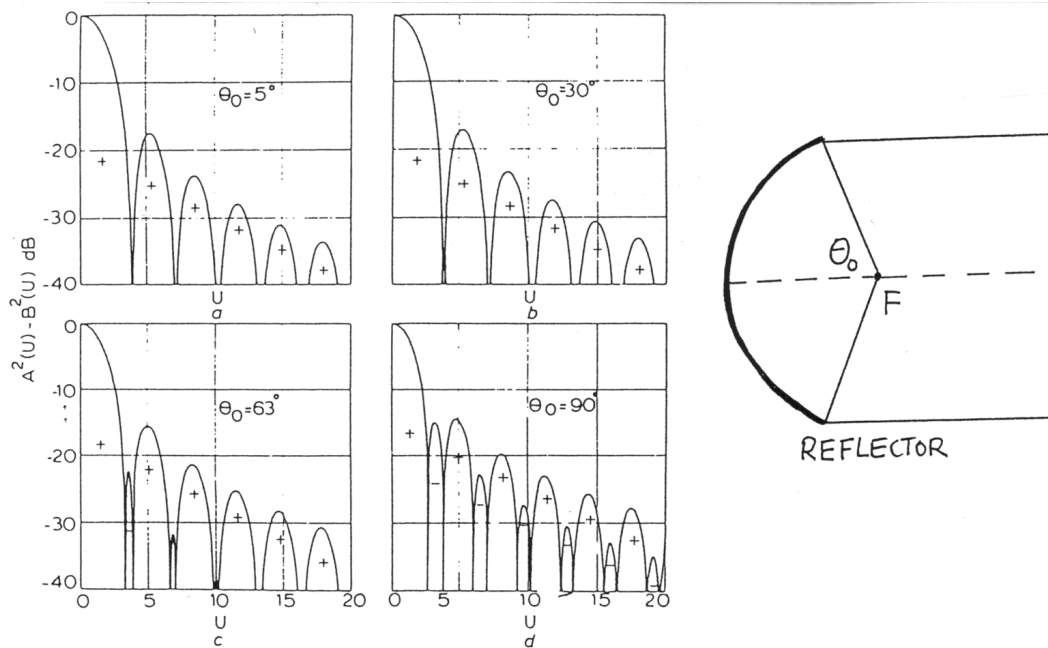


Figure 1.5: Illustration of the tapered beam pattern for telescopes using parabolic main reflectors of different steepness, expressed by the opening angle  $\theta_o$ . IRAM 30-m and 15-m telescopes:  $\theta_o \approx 63^\circ$ , optical telescopes:  $\theta_o \approx 5^\circ$ . From [Minnet & Thomas 1968], Copyright: © 1968 IEE, with kind permission from IEE Publishing Department.

p	K	$\Theta_b$ (radian)	$\Theta_{fb}$ (radian)	First sidelobe (dB)	Aperture Efficiency
0	0	$1.02 \lambda/\mathcal{D}$	$1.22 \lambda/\mathcal{D}$	17.6	1.00
1	0	$1.27 \lambda/\mathcal{D}$	$1.62 \lambda/\mathcal{D}$	24.7	0.75
2	0	$1.47 \lambda/\mathcal{D}$	$2.03 \lambda/\mathcal{D}$	30.7	0.55
1	0.25	$1.17 \lambda/\mathcal{D}$	$1.49 \lambda/\mathcal{D}$	23.7	0.87
2	0.25	$1.23 \lambda/\mathcal{D}$	$1.68 \lambda/\mathcal{D}$	32.3	0.81
1	0.5	$1.13 \lambda/\mathcal{D}$	$1.33 \lambda/\mathcal{D}$	22.0	0.92
2	0.5	$1.16 \lambda/\mathcal{D}$	$1.51 \lambda/\mathcal{D}$	26.5	0.88

Table 1.1: Beamwidths, side lobe levels, and maximum aperture efficiency ( $\epsilon_o$ ) for various parameters of the tapering function. Adapted from [Christiansen and Hogbom 1969]

with the intention to know their position, structural detail, and brightness distribution  $B_S$  as function of wavelength. The telescope thus provides information of the form

$$I(\vec{u}) \propto \int_{\text{Source}} A_T(\vec{u} - \vec{u}') B_S(\vec{u}') d\vec{u}' \quad (1.15)$$

If the telescope is perfect, and we know  $A_T$ , we can use the information  $I(\vec{u})$  to derive the calibrated brightness distribution  $B_S$  of the source distribution.

When we point the antenna toward the sky, in essence we point the beam in the direction of observation. If, for instance, we observe a point-like source it is evident that the peak of the main beam should point exactly on the source which requires that the pointing errors ( $\Delta\Theta$ ) of the telescope should be small in comparison to the beam width. The loss in gain is small, and acceptable, if the mispointing  $\Delta\Theta < 1/10 \Theta_b$ . Since modern radio telescopes use an alt-azimuth mount, this criterion says the mispointing in azimuth ( $\Delta\Theta_{az}$ ) and elevation ( $\Delta\Theta_{el}$ ) direction should not exceed  $1/\sqrt{2}$  this value. The pointing and focus (see below) of the IRAM antennas are regularly checked during an observation, and corrected if required. The corresponding protocol of an observing session at Plateau de Bure, using 5 antennas, is shown in Figure 1.6.

## 1.4 The real Single-Dish Antenna

A telescope, however, is never perfect since mechanical, thermal, and wind-induced deformations of the structure occur, and the optics may be misaligned and/or have production imperfections, for one or the other reason. The resulting effect on the beam pattern is negligible if the corresponding wavefront deformations introduced by these imperfections are small compared to the wavelength of observation, generally smaller than  $\sim \lambda/15$ ; the effect is noticeable and disturbing when the wavefront deformations are large compared to the wavelength ( $\sim 1/4\lambda$  and larger). The wavefront deformations due to such imperfections may be of systematic nature, or of random nature, or both.

### 1.4.1 Systematic Deformations: Defocus, Coma, Astigmatism

There are three basic systematic surface/wavefront deformations (occasionally associated with pointing errors) with which the observer may be confronted, i.e. defocus, coma, and astigmatism (a transient feature on the IRAM 30-m telescope).

1. The most important systematic wavefront/beam error is due to a **defocus** of the telescope. This error is easily detected, measured, and corrected from the observation of a strong source at a number of focus settings. Figure 1.7 shows, as example, the beam pattern measured on Jupiter with the telescope being gradually defocused. Evidently, the peak power in the main beam decreases, the power in the side lobes increases, until finally the beam pattern has completely collapsed. To be on

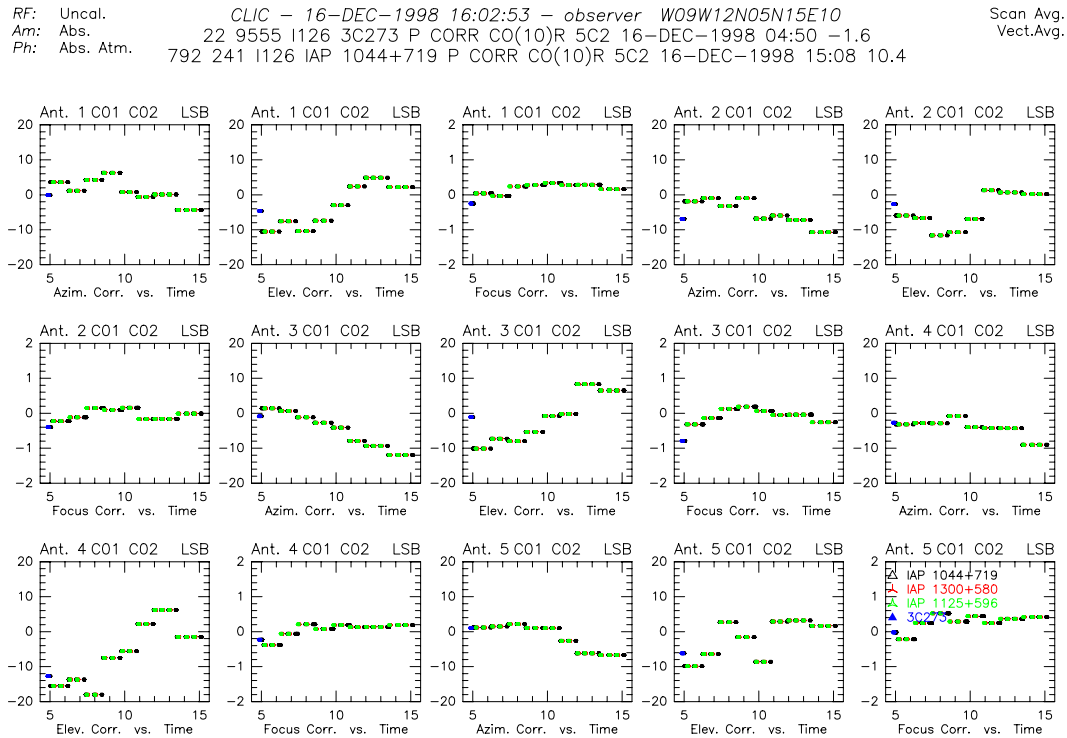


Figure 1.6: Protocol of pointing corrections applied in azimuth and elevation direction, and focus corrections; shown for 5 antennas during an observation which lasted 6 hours.

the safe side for observations, the defocus of the telescope should not exceed  $\sim 1/10\lambda$ . A defocus does *not* introduce a pointing error.

2. A telescope may have a **comatic** wavefront/beam error due to a misaligned subreflector, shifted perpendicular off the main reflector axis. Figure 8 shows, as example, a cross scan through a comatic beam of the IRAM 15-m telescope, especially produced by displacement of the subreflector. A comatic beam pattern introduces a pointing error. It may be useful for the observer to recognize this error, in particular if unexplained pointing errors occur in an observations. [The IRAM telescopes are regularly checked for misalignments, and correspondingly corrected.]
3. A telescope may have an **astigmatic** wavefront/beam error, usually introduced by complicated mechanical and/or thermal deformations (a transient feature on the IRAM 30-m telescope). While this beam deformation is easily recognized by the observer from the difference in beam widths measured from in-and-out-of-focus cross scans, the improvement of the telescope usually is difficult, and out of reach of the observer. A focused astigmatic beam does *not* introduce a pointing error. Figure 1.9 shows the focused beam pattern measured on a telescope which has a strong astigmatic main reflector (amplitude of the astigmatism  $\sim 0.5$  mm).

The beam deformation of systematic wavefront deformations occurs close to the main beam, and the exact analysis should be based on diffraction calculations. A convenient description of systematic deformations uses Zernike polynomials of order  $(n,m)$  [Born & Wolf 1975]. Without going into details, the Zernike-type surface deformation  $\delta_{n,m} = \alpha_{n,m} R_n(\rho) \cos(m\theta)$  [with  $(\rho, \theta)$  normalized coordinates of the aperture, and  $R$  special polynomial functions] with amplitude  $\alpha_{n,m}$  has a quasi rms-value  $\sigma = \alpha_{n,m}/\sqrt{n+1}$  and introduces a loss in main beam intensity of

$$\epsilon_{\text{sys}}/\epsilon_o \approx \exp[-(4\pi\alpha/\lambda)^2/(n+1)] \quad (1.16)$$

For primary coma  $n = 1$ , for primary astigmatism  $n = 2$ . Although the beam deformation may be very noticeable and severe, the associated loss in main beam intensity may still be low because of the reduction



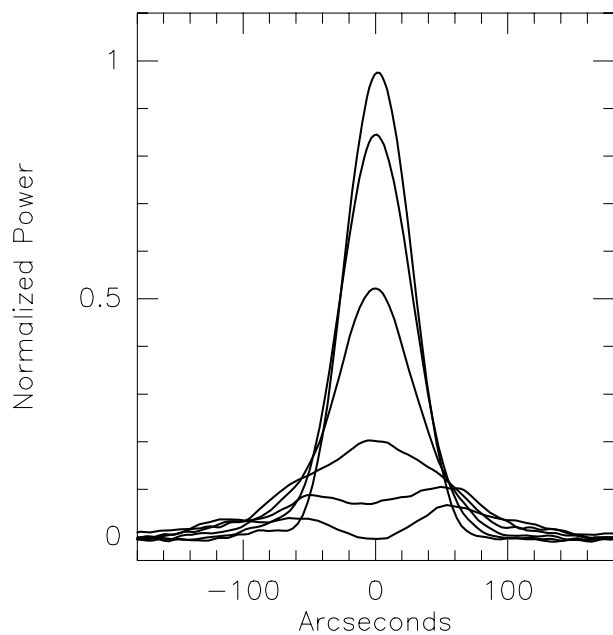


Figure 1.7: Effect on the beam pattern (scans across Jupiter) introduced by defocusing the IRAM 15-m telescope (shifts of the subreflector in steps of  $\lambda/4$ ,  $\lambda = 3$  mm).

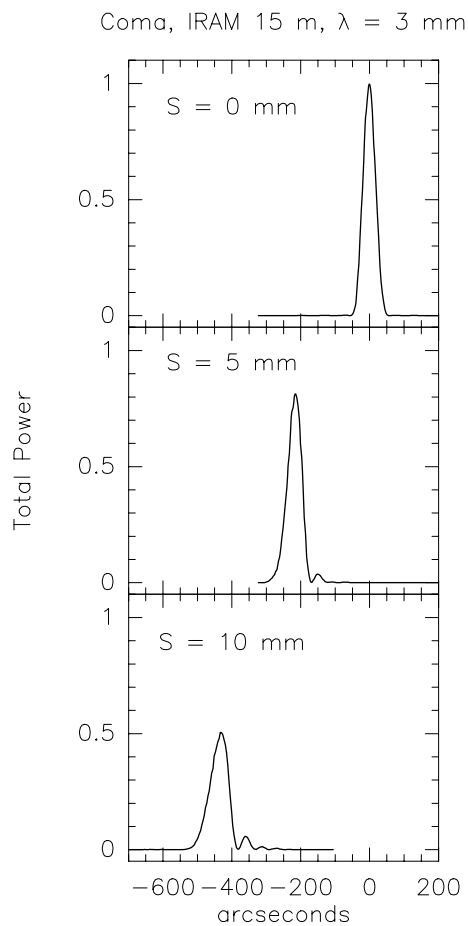


Figure 1.8: Illustration of a comatic beam (scanned in the direction of the coma) especially produced on the IRAM 15-m telescope. The shift of the subreflector is indicated by  $S$ . The beam pattern is perfect at  $S = 0$ . Note the shift of the beam (pointing error) when the subreflector is shifted.

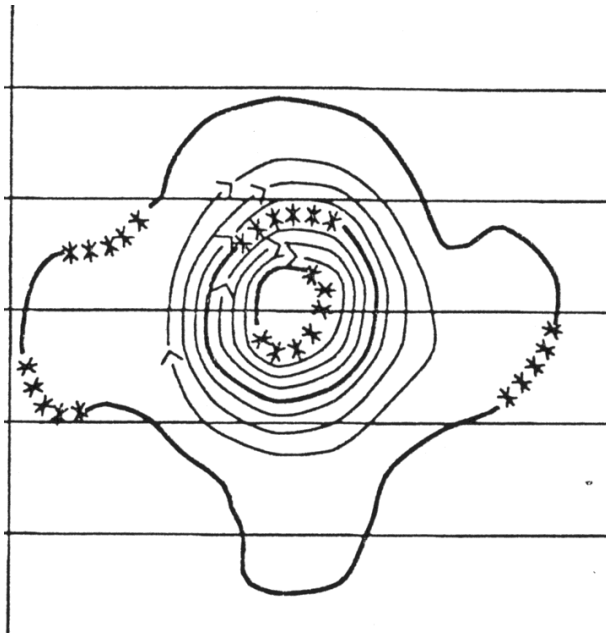


Figure 1.9: Illustration of an astigmatic beam pattern; well focused.

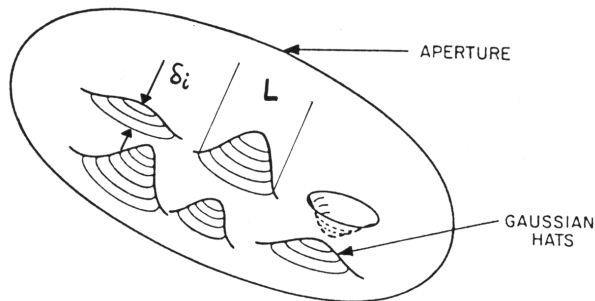


Figure 1.10: Explanation of random errors ( $\delta$ ) and their correlation length ( $L$ ), for Gaussian hat-like deformations (example). From [Ruze 1966], Copyright: © 1966 IEEE, reprinted by permission of IEEE, Inc.

by the factor  $(n+1)$ .

### 1.4.2 Random Errors

Besides systematic surface/wavefront deformations explained above (mainly due to misalignment of the optics), there are often permanent random deformations on the optic surfaces like ripples, scratches, dents, twists, misaligned panels, etc., with spatial dimensions ranging from several wavelengths to significant areas of the aperture. These deformations introduce identical deformations of the wavefront, which cannot be expressed in mathematical form (as the Zernike polynomials used above). Nevertheless, the effect on the beam pattern of this type of deformations can be analyzed in a statistical way and from a simple expression, the RUZE equation. This equation is often used to estimate the quality of a telescope, in particular as function of wavelength. The values obtained from this equation are directly related to the aperture efficiency, and beam efficiency, of the telescope, and hence are important for radiometric measurements (see Sect.1.5).

As illustrated in Figure 1.10, there are two parameters which allow a physical-optics description of the influence of random errors, i.e. the rms-value (root mean square value)  $\sigma$  of the deformations, and their correlation length  $L$ .

Random errors occur primarily on the main reflector; the other optical components of the telescope (subreflector, Nasmyth mirror, lenses, polarizers) are relatively small and can be manufactured with good precision. In order to explain the rms-value  $\sigma$ , we assume that the reflector aperture is divided into *many* elements ( $i = 1, 2, \dots, N$ ), and that for each element  $[i]$  the deformation  $\delta(i)$  of the reflector is known with

respect to a smooth mean surface. The rms-value of these random surface deformations is

$$\sigma = \sqrt{\sum_{i=1,N} \delta(i)^2 / N} \quad (1.17)$$

The surface deformations  $\delta(i)$  introduce corresponding wavefront deformations  $\varphi(i)$ , approximately two times larger than the mechanical deformations  $\delta$  in case we are dealing with reflective optics. The rms-value  $\sigma_\varphi$  of the corresponding phase deformations of the wavefront is

$$\sigma_\varphi = 2 k R \sigma \quad (1.18)$$

again with  $k = 2\pi/\lambda$ , and  $R \approx 0.8$  a factor which takes into account the steepness of the parabolic main reflector [Greve & Hooghoudt 1981].

A description of the wavefront deformation by the rms-value  $\sigma_\varphi$  is incomplete since the value does not contain information on the structure of the deformations, for instance whether they consist of many dents at one part of the aperture, or many scratches at another part. A useful physical-optics description requires also a knowledge of the correlation length  $L$  of the deformations.  $L$  is a number ( $L \leq \mathcal{D}$ ) which quantifies the extent over which the randomness of the deformations does not change. For example, the deformations of a main reflector constructed from many individual panels, which may be misaligned, often has a random error correlation length typical of the panel size, but also a correlation length of 1/3 to 1/5 of the panel size due to inaccuracies in the fabrication of the individual panels. A typical example is the 30-m telescope [Greve et al. 1998].

When knowing, by one or the other method, the rms-value  $\sigma_\varphi$  and the correlation length  $L$ , it is possible to express the resulting beam shape in an analytic form which describes well the real situation. The beam pattern  $\mathcal{F}(\times)$  of a wavefront with random deformations ( $\sigma_\varphi, L$ ) [the telescope may actually have several random error distributions] consists of the degraded diffraction beam  $\mathcal{F}_c(\times)$  and the error beam  $\mathcal{F}_e(\times)$  such that

$$\mathcal{F}(\Theta) = \mathcal{F}_c(\Theta) + \mathcal{F}_e(\Theta) \quad (1.19)$$

with

$$\mathcal{F}_c(\Theta) = \exp[-(\sigma_\varphi)^2] A_T(\Theta) \quad (1.20)$$

where  $A_T(\Theta)$  is the tapered beam pattern (Eq.1.14), and

$$\mathcal{F}_e(\Theta) = a \exp[-(\pi\Theta L/\lambda)^2] \quad (1.21)$$

where

$$a = (L/\mathcal{D})^2 [1 - \exp(-\sigma_\varphi^2)] / \epsilon_o \quad (1.22)$$

In these equations,  $\mathcal{D}$  is the diameter of the telescope aperture,  $\lambda$  the wavelength of observation,  $\Theta$  the angular distance from the beam axis, and  $\epsilon_o$  the aperture efficiency of the perfect telescope. In the formalism used here the beam is circular symmetric. The error beam  $\mathcal{F}_e(\times)$  has a Gaussian profile of width FWHP)  $\Theta_e = 0.53\lambda/L$  [radians], i.e. the smaller the correlation length (the finer the irregular structure), the broader is the beam width  $\Theta_e$ . The random errors of panel surface deformation and panel alignment errors may have large error beams (up to arcminutes in extent) which can pick up radiation from a large area outside the actual source. A knowledge of the structure and of the level of the error beam(s) is therefore important when mapping a source and making absolute power measurements. Figure 1.11 shows the diffraction beam and the combined error patterns measured on the 30-m telescope at various wavelengths. The smaller the wavelength of observation, the smaller is the power received in the main beam and the larger the power received in the error beam. Due to its particular mechanical construction, this telescope has three error beams [Greve et al. 1998].

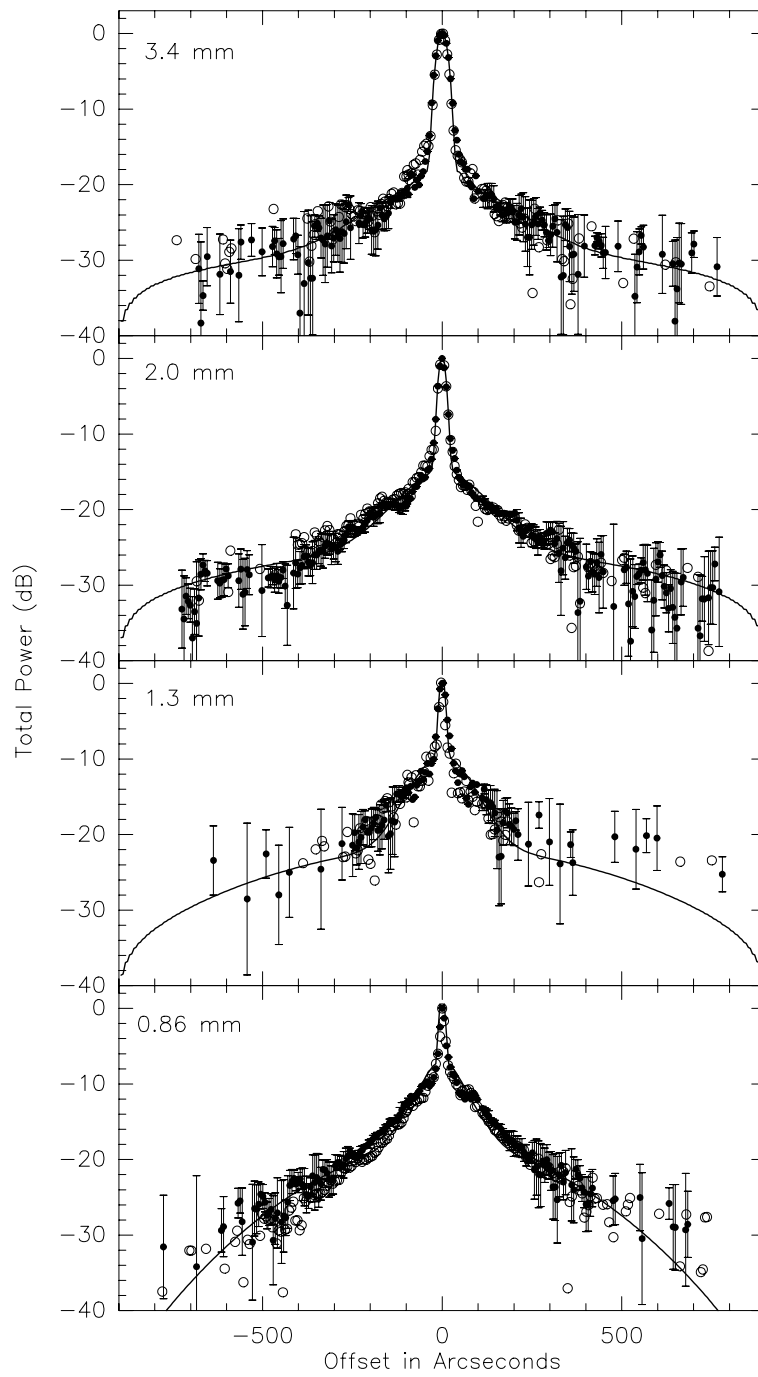


Figure 1.11: Beam pattern measured on the IRAM 30-m telescope. The beam consists of the diffraction beam ( $\approx$  main beam) and a combined, extended error beam (solid line).

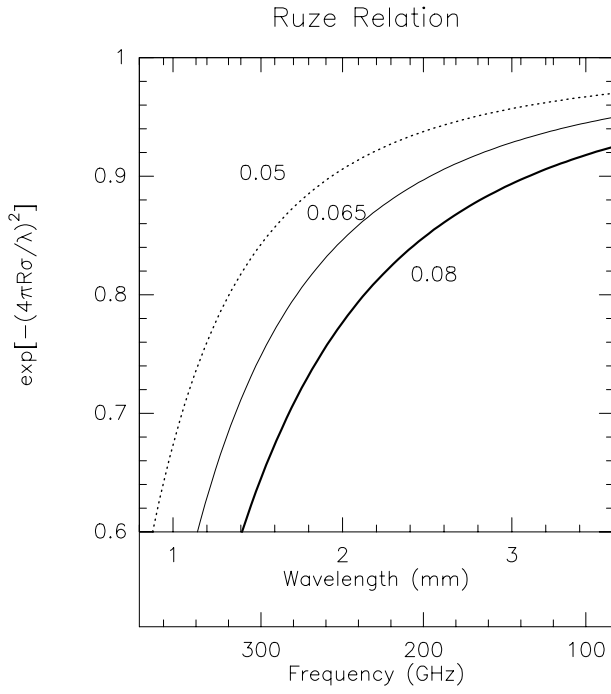


Figure 1.12: Illustration of the RUZE relation  $\exp[-(4\pi R\sigma/\lambda)^2]$  as function of wavelength (frequency) and values  $R\sigma$  as indicated (mm).

## 1.5 Radiometric Relations

The imperfections of a telescope, either due to systematic or random errors, produce beam deformations, a loss in gain, and focus and pointing errors. These effects must be taken into account when mapping and measuring a source. Information on the beam pattern obtained from a map (for instance holography map) of a strong point-like source; information on the sensitivity [Jy/K] and calibration of the telescope is obtained from absolute power measurements of, for instance, the planets, of which the brightness temperatures are quite well known. This information is usually collected by the observatory staff, and provided to the observer (30-m Telescope Manual; observation protocols of Plateau de Bure measurements).

We summarize the influence of random deformations, at least as far as the main beam is concerned, since for this case the RUZE equation provides sufficient precision for an understanding of the telescope behaviour; also for the astronomer observer without going into complicated radio optics detail. This relation appears in the expression of the diffraction beam  $\mathcal{F}_c$  (see Eq.1.20) and shows clearly the fact that the degradation of the telescope, in particular for power measurements, increases exponentially with wavelength.

### Aperture Efficiency:

$$\epsilon_{ap} = \epsilon_o \exp[-\sigma_\varphi] = \epsilon_o \exp[-(4\pi R\sigma/\lambda)^2]$$

### Antenna Gain:

$$S/T_A^* = 2(k/A)\eta_f/\epsilon_{ap} \approx 2(k/A) \exp[+(4\sigma R/\lambda)^2]/\epsilon_{ap} \quad [\text{Jy/K}]$$

### Beam Efficiency:

$$\begin{aligned} \eta_b &= 0.8899 [\Theta_b/(\lambda/D)]^2/\epsilon_{ap} \\ \Theta_b &= \alpha\lambda/D, \quad 1 \leq \alpha \leq 1.2 \quad [\text{radians}] \\ \eta_b &\approx 1.2 \epsilon_o \exp[-(4\pi R\sigma/\lambda)^2] \end{aligned}$$

The quantities in these expressions are  $\epsilon_o$ : aperture efficiency of the perfect telescope (usually of the order of  $\sim 75 - 90\%$ ; see Table 1.1);  $\epsilon_{ap}$ : effective aperture efficiency at the wavelength  $\lambda$ , including all wavefront / telescope deformations;  $\sigma$ : rms-value of the telescope optics deformations;  $R \approx 0.8$ : reduction factor for a steep main reflector ( $N = F/D \approx 0.3$ );  $S$ : flux density of a point source [Jy];  $T_A^*$ : measured antenna temperature [K] (see also Chapter 10);  $A$ : geometric surface area of the telescope [ $\text{m}^2$ ];  $\eta_f$ : forward efficiency, measured at the telescope for instance from a sky dip;  $\Theta_b$ : main beam width (FWHP).

